

## ULTRA-HIGH-DENSITY MOLECULAR CORE AND WARPED NUCLEAR DISK IN THE DEEP POTENTIAL OF RADIO LOBE GALAXY NGC 3079

Y. SOFUE,<sup>1</sup> J. KODA,<sup>1</sup> K. KOHNO,<sup>2</sup> S. K. OKUMURA,<sup>2</sup> M. HONMA,<sup>3</sup> A. KAWAMURA,<sup>1</sup> AND JUDITH A. IRWIN<sup>4</sup>

Received 2000 September 5; accepted 2000 November 15; published 2001 January 24

### ABSTRACT

We have performed high-resolution synthesis observations of the  $^{12}\text{CO}$  ( $J = 1-0$ ) line emission from the radio lobe edge-on spiral galaxy NGC 3079 using a seven-element millimeter-wave interferometer at the Nobeyama Radio Observatory, which consisted of the 45 m telescope and six-element array. The nuclear molecular disk (NMD) of 750 pc radius is found to be inclined by  $20^\circ$  from the optical disk, and the NMD has spiral arms. An ultra-high-density core (UHC) of molecular gas was found at the nucleus. The gaseous mass of the UHC within 125 pc radius is as large as  $\sim 3 \times 10^8 M_\odot$ , an order of magnitude more massive than that in the same area of the Galactic center, and the mean density is as high as  $\sim 3 \times 10^3 \text{ H}_2 \text{ cm}^{-3}$ . A position-velocity diagram along the major axis indicates that the rotation curve already starts at a finite velocity exceeding  $300 \text{ km s}^{-1}$  from the nucleus. The surface mass density in the central region is estimated to be as high as  $\sim 10^5 M_\odot \text{ pc}^{-2}$ , producing a very deep gravitational potential. We argue that the very large differential rotation in such a deep potential will keep the UHC gravitationally stable during the current star formation.

*Subject headings:* galaxies: individual (NGC 3079) — galaxies: ISM — galaxies: kinematics and dynamics — galaxies: nuclei — ISM: molecules — radio lines: ISM

### 1. INTRODUCTION

NGC 3079 is an edge-on galaxy known for its pronounced radio,  $\text{H}\alpha$ , and X-ray lobes emerging from the nucleus (Hummel, van Gorkom, & Kotanyi 1983; Duric, Seaquist, & Davis 1983; Ford et al. 1986; Veilleux et al. 1994; Pietsch, Trinchieri, & Vogler 1998). The nuclear outflow may originate with the accretion of dense gas onto a compact core (Irwin & Seaquist 1988), and the nucleus exhibits LINER and Seyfert 2 nuclear activity (Ford et al. 1986). NGC 3079 has been studied in various radio wave bands in continuum,  $\text{H I}$ , and CO lines as well as maser lines (Irwin & Seaquist 1988, 1991; Ford et al. 1986; Duric et al. 1983; Duric & Seaquist 1988; Irwin et al. 1987; Young, Claussen, & Scoville 1988; Sofue & Irwin 1992; Irwin & Sofue 1992; Braine et al. 1997; Sawada-Sato et al. 2000). The galaxy's distance is 15.6 Mpc ( $H_0 = 75 \text{ km s}^{-1} \text{ Mpc}^{-1}$ ), the major-axis position angle (P.A.) of the optical disk is  $167^\circ$ , and the inclination angle is  $85^\circ$ .

Earlier CO observations with the Nobeyama Millimeter Array (NMA) inferred the existence of a dense nuclear molecular disk rotating at a high velocity within the central  $10''$  (750 pc; Sofue & Irwin 1992; Irwin & Sofue 1992). NGC 3079 is a galaxy whose unusual nuclear activity can be probed by observing the affected interstellar medium (ISM) and can be compared with the Milky Way for its similar edge-on orientation. Knowledge of the kinematics, morphology, and density of the ISM in the immediate vicinity of the nucleus is particularly important since the ISM can both fuel the nucleus and trigger activity. The nuclear disk could also play a role in collimating outflows. For this, higher resolution CO observations have been required to determine how the morphology and kinematics of the nuclear molecular disk are related to the nuclear activity.

In this Letter, we report the result of high-resolution CO line observations of NGC 3079 using a seven-element millimeter-wave interferometer at the Nobeyama Radio Observatory (NRO) by combining the NMA and the 45 m telescope, whose code name was “RAINBOW.”

### 2. OBSERVATIONS

The  $^{12}\text{CO}$  ( $J = 1-0$ ) observations of NGC 3079 were made on 2000 January 18 and February 2 in the seven-element RAINBOW mode at NRO, which consisted of six 10 m antenna arrays in an AB configuration linked with the 45 m telescope. Observations in the C- and D-configuration observations were made on 2000 March 12 and April 12, respectively. The  $u-v$  coverage of the observations was ideal for the high declination. After obtaining UV data for individual array configurations, they were combined, and data analysis was done by using the AIPS standard packages. The UV data were CLEANed and Fourier-transformed to three-dimensional cubes in right ascension, declination, and frequency space, and they were further transposed to (R.A., decl.,  $V_{\text{LSR}}$ )-cubes. The synthesized half-power beamwidth was  $1''.62 \times 1''.34$ , slightly elongated in the direction of P.A. =  $110^\circ$ , for combined UV data of the seven-element synthesis in AB, C, and D configurations (RABCD configuration). The beam for the seven-element AB configuration without C and D was  $1''.27 \times 1''.09$  elongated at P.A. =  $106^\circ$  (RAB configuration). At a distance of 15.6 Mpc,  $1''$  corresponds to 75 pc.

The center position of the galaxy was taken at the radio nucleus at R.A. =  $09^{\text{h}}58^{\text{m}}35^{\text{s}}.02$  and decl. =  $55^\circ55'15''.4$  (epoch 1950), and the systemic LSR velocity was taken as  $1113 \text{ km s}^{-1}$ . The phase and bandpass calibrations were made by observing the nearby radio source QSO 0957+561, which was measured and found to have a flux density of 0.68 Jy at the observing frequency for the RAB array in 2000 January and February and of 0.58 Jy for the C and D arrays in 2000 March and April. The field of view for the seven-element array, including the 45 m telescope (RABCD), was  $20''$ , and that for the six-element ABCD-configuration array without the 45 m telescope was  $60''$ .

<sup>1</sup> Institute of Astronomy, University of Tokyo, Mitaka, Tokyo, 181-0015, Japan; sofue@ioa.s.u-tokyo.ac.jp

<sup>2</sup> Nobeyama Radio Observatory, National Astronomical Observatory (NAO) of Japan, 2-21-1, Osawa, Mitaka, Tokyo, 181-8588, Japan.

<sup>3</sup> VERA Project Office, NAO, Mitaka, Tokyo, 181-8588; and Mizusawa Astrodynamics Observatory, NAO, Mizusawa, 023-0861, Japan.

<sup>4</sup> Department of Physics, Queen's University, Kingston, Ontario, K7L 3N6, Canada.

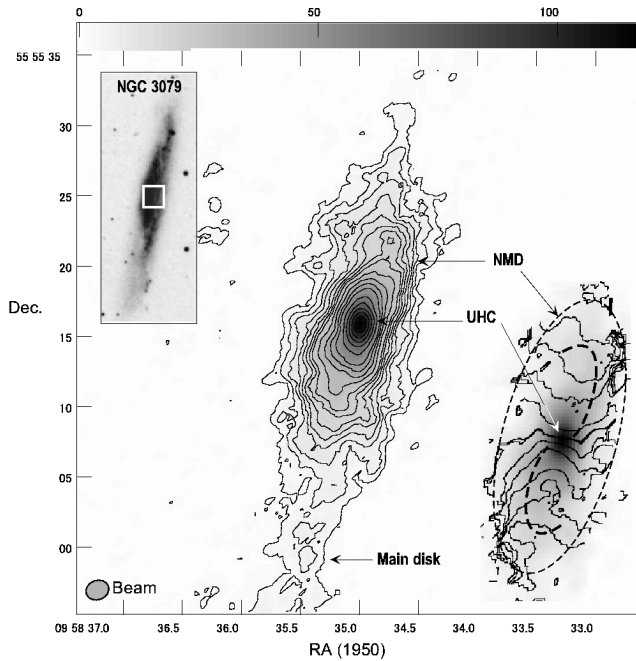


FIG. 1.—Distribution of integrated intensity of the  $^{12}\text{CO}$  ( $J = 1-0$ ) line emission in the central  $40'' \times 40''$  area of NGC 3079. The angular resolution is  $1''.62 \times 1''.36$ . A UHC is embedded in the NMD, which is further surrounded by the main disk component (arrows). Contours are at 2.5%, 25%, 50%, ..., 100% of the peak intensity. The lower right inset is a mean velocity field. The thick velocity contour near the center is at  $1100 \text{ km s}^{-1}$ , and the contours are drawn at  $50 \text{ km s}^{-1}$  increments, increasing toward the south. The thin dashed ellipse outlines the NMD. Two molecular spiral arms are traced by the thick dashed lines. The upper left inset is a  $B$ -band image from the Palomar Digital Sky Survey (vertical extent  $8'$ ). The small white box indicates the CO map region.

This yielded a higher sensitivity in the central  $20''$  region than in the surrounding region.

Figure 1 shows the integrated intensity map of the CO line from the RABCD configuration, and a mean velocity field at a resolution of  $1''.62 \times 1''.36$  is shown as an inset. The major structures discussed below are illustrated by the arrows and the dashed contours. A  $B$ -band image from the Palomar Digital Sky Survey is shown as an inset in the upper left-hand corner. Figure 2 shows the integrated intensity for the central region from the RAB configuration with a higher resolution of  $1''.27 \times 1''.09$ . Figure 3 shows position-velocity (PV) diagrams along the major axis with a  $5''$  slit width by the RABCD array (*upper panel*) and for the innermost region with a  $2''$  slit width by the RAB array (*lower panel*).

### 3. MOLECULAR STRUCTURES

#### 3.1. Ultra-High-Density Molecular Core

The most remarkable feature in the intensity maps (Figs. 1 and 2) is a very compact, intense CO concentration at the nucleus. This “ultra-high-density core” (UHC) of molecular gas is elongated in the north-south direction at P.A. =  $176^\circ$ , inclined by  $9^\circ$  from the main disk. The FWHM of the UHC is measured to be  $3''.3 \times 1''.8$  (250 pc  $\times$  180 pc), and therefore the radius is about 125 pc.

The integrated CO intensity at the nucleus is  $117 \text{ Jy beam}^{-1} \text{ km s}^{-1}$ , or  $I_{\text{CO}} = 5.0 \times 10^3 \text{ K km s}^{-1}$ . The  $\text{H}_2$  column density toward the nucleus is estimated to be  $N_{\text{H}_2} \sim 5.0 \times 10^{23} \text{ H}_2 \text{ cm}^{-2}$ , where we took a conversion factor for the centers of gal-

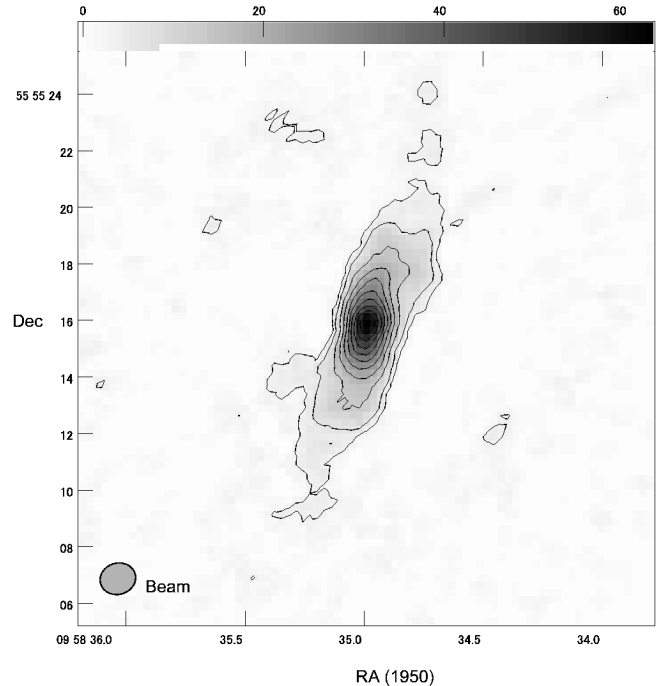


FIG. 2.—Central  $20'' \times 20''$  at a higher resolution of  $1''.27 \times 1''.09$ . The UHC shows up more clearly. Contours are at 5%, 10%, 20%, ..., 100% of the peak intensity.

axies of  $X = 1.0 \times 10^{20} \text{ H}_2 \text{ K}^{-1} (\text{km s}^{-1})^{-1}$  (Arimoto, Sofue, & Tsujimoto 1996).

The total molecular mass in the UHC is estimated to be  $M_{\text{gas}} = 3 \times 10^8 M_\odot$ . Since the vertical direction is not resolved, we here assume that the thickness of the UHC is of the same order of 30 pc as the molecular ring in the Milky Way center (Sofue 1995). Then the mean density of molecular hydrogen is estimated to be on the order of or higher than  $\sim 3 \times 10^3 \text{ H}_2 \text{ cm}^{-3}$ . Hence, the UHC consists of a pile of molecular gas equivalent to a 1000 medium-sized giant molecular clouds within a 125 pc radius.

The velocity field in Figure 1 (*lower right inset*) shows that the UHC is rotating regularly but very rapidly. The PV diagrams (Fig. 3) show that the rotation velocity in the central  $1''$  region rises extremely steeply, or more likely the velocity starts at a finite velocity of  $\sim 300 \text{ km s}^{-1}$  already at the nucleus. We may estimate the dynamical mass from the rotation velocity because the pressure term due to the velocity dispersion is negligible for Population I gases, particularly for molecular gas. The dynamical mass within  $R = 125 \text{ pc}$  is then estimated to be  $M_{\text{dyn}} = V_{\text{rot}}^2 R/G \sim 2 \times 10^9 M_\odot$ . Hence, the gaseous mass in the molecular core shares about 15% of the dynamical mass.

#### 3.2. Warped Nuclear Disk with Spiral Arms

The molecular core is surrounded by the nuclear molecular disk (NMD) of radius  $10''$  (750 pc) elongated in the direction of the optical major axis (Fig. 1, *dashed ellipse*). The projected minor-to-major axial ratio of the ellipse is as large as 0.40. Since the disk thickness is considered to be sufficiently small, such a fat shape indicates that the inclination angle of the disk is  $66^\circ$ . This implies that the NMD is not in the same plane as the outer optical disk whose inclination angle is  $85^\circ$ . The NMD is therefore warped by about  $20^\circ$  from the main optical disk.

The disk is superposed by two symmetrical spiral arms, one arm extending from the northwest of the UHC toward the north

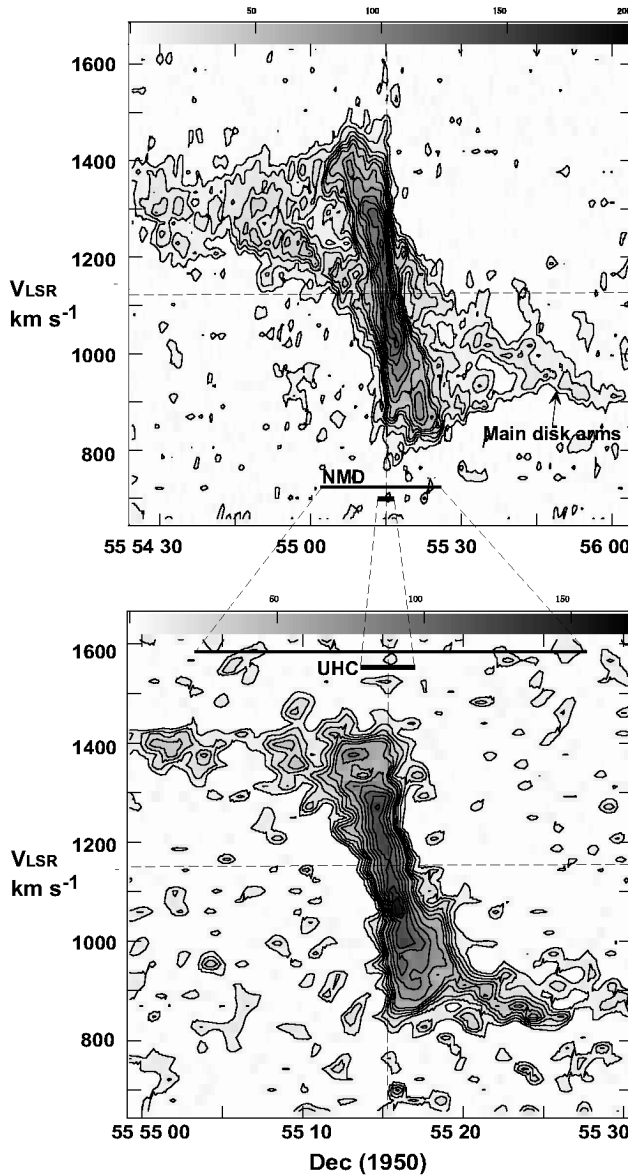


FIG. 3.—Upper panel: PV diagram along the major axis of NGC 3079 in CO with a slit width of 5'' (original resolution 1''.62 × 1''.34). Contours are at 5%, 10%, 20%, ..., 100% of the peak intensity. The lower panel shows the same, but for the central region at a higher resolution with a slit width of 2'' (original resolution 1''.27 × 1''.09).

and the other from southeast to the south, that are illustrated by dashed lines in the inset of Figure 1. If we assume that the spiral arms are trailing, the eastern half of the disk is on the far side, and the western half is near side. This configuration is in the same sense as that of the outer optical disk.

The velocity field shows that the circular rotation is dominant. The slightly distorted velocity field is superposed, which suggests a small noncircular motion that is due to spiral arms. Since the intensity map shows spiral arms, the latter may be more likely. In the PV diagram, the spiral arms show up as inclined ridges in the central 10'', crossing the bright ridge of the UHC.

The total mass of molecular gas of the NMD, including the outskirt extending to radius 900 pc, is estimated to be  $2 \times 10^{10} M_{\odot}$  for the same conversion factor as above. This shares about 14% of the dynamical mass within the same radius,

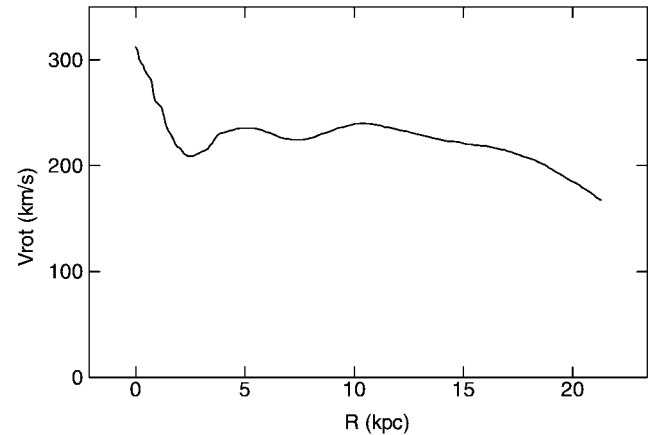


FIG. 4.—Rotation curve of NGC 3079

$1.4 \times 10^{10} M_{\odot}$ , for a rotation velocity of 260 km s<sup>-1</sup> at 900 pc radius.

### 3.3. Main Disk

Figure 1 indicates the existence of a more extended, narrower component that is extended in the direction of the optical major axis for more than  $\pm 30''$  ( $\pm 2.2$  kpc). This feature is attributed to the outer main disk visible in optical images associated with dust lanes. This disk component is slightly lopsided in the sense that the southern part is brighter.

The disk also shows up in the PV diagram (Fig. 3) as the two symmetrical tilted ridges crossing the UHC and NMD. Such PV ridges are typical for grand-design two-armed density-wave spirals. These PV ridges are bifurcated from the maximum-velocity parts of the PV ridges because of the NMD. Hence, these disk arms may be continued to the spiral arms in the NMD.

### 4. ROTATION CURVE AND MASS DISTRIBUTION

Applying the envelope-tracing method (Sofue 1996) to the PV diagrams, we have derived a rotation curve and combined it with an outer rotation curve obtained from H I data (Irwin & Seaquist 1991). The obtained rotation curve for the entire galaxy is shown in Figure 4. The rotation curve already starts from a very high finite value in the nucleus, followed by the usual curve in the disk and halo. High velocities in the center, followed by a flat rotation in the disk and halo, exhibiting a broad maximum in the disk, are commonly found in spiral galaxies observed with sufficiently high resolutions (Sofue et al. 1999).

Since the circular motion is dominant (Fig. 1), we then use the rotation curve to calculate directly the distribution of the surface mass density (SMD), applying the method developed by Takamiya & Sofue (2000). Figure 5 shows the obtained SMD, where the thick line shows the result for a flat-disk assumption, and the thin line for a spherical assumption (see Takamiya & Sofue 2000 for details). The true SMD value is considered to be sandwiched by the two lines (thick and thin) within an error of about 30%, except for the outermost region, where the edge effect becomes not negligible. The SMD between  $R \sim 1$  and 8 kpc is well fitted by an exponential disk of a scale (e-folding) radius of 3.5 kpc. The bulge component between 0.3 and 1 kpc can be approximated by an  $\sim e^{-(R/200 \text{ pc})^{1/4}}$  law. The innermost region within  $R \sim 300$  pc shows a much steeper increase toward the nucleus, exhibiting an extremely high density dynamical core with an SMD as high as  $10^5 M_{\odot} \text{ pc}^{-2}$  at  $R \sim 100$  pc.

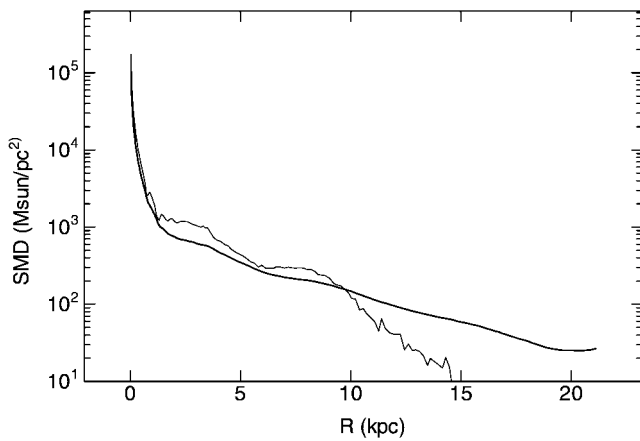


FIG. 5.—SMD plotted against radius. The thick curve is the result of a flat-disk assumption; the thin line is the result of a spherical assumption.

## 5. DISCUSSION

The central  $R \sim 100$  pc region of NGC 3079 is filled with the UHC with a molecular mass as high as  $3 \times 10^8 M_{\odot}$ . The UHC is rotating regularly at a high speed of  $\sim 300$  km s $^{-1}$  in the deep gravitational potential. The molecular gas density and mass are an order of magnitude greater than those in the Galactic center. We stress that such an extremely high density massive interstellar condition was found for the first time.

Here we consider the reason why such a dense core could have survived in the gas phase without suffering from the current star formation. The Jeans time in the UHC is on the order of  $t_J \sim 10^6$  yr. On the other hand, the dynamical timescale for a cloud to be torn off by the Coriolis force and differential rotation is  $t_D \sim dV/dR - \omega \sim 2.5 \times 10^5$  yr. Here  $V$ ,  $R$ , and  $\omega$

are the rotation velocity, radius, and angular velocity, respectively. Hence,  $t_J > t_D$ , so that clouds cannot collapse to form stars but are kept gravitationally stable and stretched azimuthally along the orbits by the differential rotation. Velocity dispersion would be an alternative cause for the suppression of star formation. However, the random motion and turbulence in molecular gas are known to be several kilometers per second or less, which will affect the stability compared with the effect of the high differential rotation a lot less.

Formation of the UHC could be understood as being due to the accretion by noncircular streaming motion from the NMD, as readily suggested from the spiral pattern in the NMD. The existence of a compact, massive central mass would cause the rapid accretion of the disk gas to a dense core in circular rotation, as is indeed simulated by Fukuda, Habe, & Wada (2000).

Another important finding is that both the NMD and the UHC are significantly warped from the main disk. The warp of NMD may explain why the H $\alpha$  lobe is highly asymmetric or lopsided (Veilleux et al. 1994). The warping of the central gas disks does not appear to be a rare case. In fact, Schinnerer et al. (2000) have shown by their high-resolution interferometer observations in the CO line that the nuclear molecular disk of the Seyfert galaxy NGC 1068 is significantly warping. We finally mention that the origin of the highly inclined nuclear torus of a few parsec scales, as inferred from VLBI jet directions (Irwin & Seaquist 1988) and maser spots (Sawada-Satoh et al. 2000), could be somehow related to the warp of its progenitor, NMD and UHC, from which the torus had accreted.

The authors thank the NRO staff for helping us in the observations. They also thank T. Takamiya for the program to calculate the surface mass density from rotation curves.

## REFERENCES

- Arimoto, N., Sofue, Y., & Tsujimoto, T. 1996, PASJ, 48, 275  
 Braine, J., Guelin, M., Dumke, M., Brouillet, N., Herpin, F., & Wielebinski, R. 1997, A&A, 326, 963  
 Duric, N., & Seaquist, E. R. 1988, ApJ, 326, 574  
 Duric, N., Seaquist, E. R., & Davis, L. E. 1983, ApJ, 273, L11  
 Ford, H. C., Dahari, O., Jakoby, G. H., Crane, P. C., & Carduloo, R. 1986, ApJ, 311, L7  
 Fukuda, H., Habe, A., & Wada, K. 2000, ApJ, 529, 109  
 Hummel, E., van Gorkom, J. H., & Kotanyi, C. G. 1983, ApJ, 267, L5  
 Irwin, J. A., & Seaquist, E. R. 1988, ApJ, 335, 658  
 ———. 1991, ApJ, 371, 111  
 Irwin, J. A., Seaquist, E. R., Taylor, A. R., & Duric, N. 1987, ApJ, 313, L91  
 Irwin, J. A., & Sofue, Y. 1992, ApJ, 396, L75  
 Pietsch, W., Trinchieri, G., & Vogler, A. 1998, A&A, 340, 351  
 Sawada-Satoh, S., Inoue, M., Shibata, K. M., Kameno, S., Migenes, V., Nakai, N., & Diamond, P. J. 2000, PASJ, 52, 421  
 Schinnerer, E., Eckart, A., Tacconi, L. J., Genzel, R., & Downes, D. 2000, ApJ, 533, 850  
 Sofue, Y. 1995, PASJ, 47, 527  
 ———. 1996, ApJ, 458, 120  
 Sofue, Y., & Irwin, J. A. 1992, PASJ, 44, 353  
 Sofue, Y., Tutui, Y., Honma, M., Tomita, A., Takamiya, T., Koda, J., & Takeda, Y. 1999, ApJ, 523, 136  
 Takamiya, T., & Sofue, Y. 2000, ApJ, 534, 670  
 Veilleux, S., Cecil, G., Bland-Hawthorn, J., Tully, R. B., Filippenko, A. V., & Sargent, W. L. W. 1994, ApJ, 433, 48  
 Young, J. S., Claussen, M. J., & Scoville, N. Z. 1988, ApJ, 324, 115